Isotopic Imaging using fs-LA single collector ICP-SFMS for direct U/Th dating of small archaeological carbonates

Loïc Martin[1,2,3*], Asmodée Galy[1,2], Gaëlle Barbotin[1], Fanny Claverie[1], Edwige Pons-Branchu[3], Chantal Tribolo[2], Norbert Mercier[2], Christophe Pécheyran[1*]

1. Universite de Pau et des Pays de l'Adour, E2S UPPA, CNRS, IPREM, Avenue de l'Université, BP 576 64012 PAU cedex, France

2. IRAMAT-CRP2A, Université Bordeaux Montaigne, CNRS : UMR 5060, Esplanade des Antilles 33607 Pessac Cedex, France

3. LSCE/IPSL, UMR 8212, CEA-CNRS-UVSQ, Université Paris-Saclay, Chemin de Saint Aubin - RD 128, F-91191 Gif sur Yvette Cedex, France

ABSTRACT: We present a new methodology for the U/Th dating of carbonate materials using femtosecond laser ablation single collector inductively coupled plasma sector field mass spectrometry (fsLA single collector ICP-SFMS), isotopic mappings and image processing. This approach allows working on samples at very low U levels (ng.g^{-1}). One of the major advantages of this imaging method is that it allows to exploit deteriorated samples that could not be analyzed by conventional bulk U/Th dating methods, thanks to the identification of contaminated or leached areas at the scale of a few tens of microns and the subsequent correction for detrital ^{230}Th incorporation. Only a few milligrams of material are required for measurement, which permits to work on small samples such as shell fragments. The parameters of the fsLA-single collector ICP-SFMS coupling have been carefully optimized to ensure very high sensitivity detection and ultra-low background while preserving good plasma robustness and a spatial resolution of 30x50 µm^2. The accuracy was evaluated from low level U speleothems previously dated by a conventional U/Th dating technique involving digestion, resin purification, double spike, and detection by multicollector inductively coupled plasma mass spectrometry (MC-ICPMS). U/Th ages of two archaeological samples with U at the low ng.g^{-1} levels, a giant terrestrial snail shell and a burnt ostrich eggshell, were determined. The measured U/Th ages are consistent with the expected ages determined by luminescence dating methods.

For decades, the U/Th dating of carbonates has been widely used to establish the chronology of archaeological and geological sequences, ranging from a few years to about 600 ka, with a good accuracy[1]. Besides, carbonates of different natures (likes speleothems or shells) are commonly found in many prehistoric sites worldwide, which makes this method so important for archaeology.

Age determination using the U/Th geochronometer requires accurate measurement of the isotope ratios ^{230}Th/^{234}U and ^{234}U/^{238}U in order to solve the age equation (Supporting Information, Formula S-1). The conventional approach requires sample digestion, uranium and thorium (respectively noted U and Th in the following) extraction using ion exchange resins and isotope dilution followed by mass spectrometry analysis using either thermal ionization mass spectrometry (TIMS)[1], or, more recently, multicollector inductively coupled plasma mass spectrometry (MC-ICPMS)[2]. In the following, this approach is named the "conventional approach". Due to the low U-series content of most archaeological shells (that can be as low as a few tens of ng.g^{-1} or less of ^{238}U, and then lead to a few hundredths of fg.g^{-1} of ^{230}Th depending on the age), the conventional approach usually requires at least one hundred milligrams of material to produce ages with an accuracy of a few percent at the 95% confidence level (95% CL). This difficulty is compounded by the fact that carbonates can be subjected to detrital incorporation of U and Th isotopes: ^{230}Th and ^{234}U atoms that do not result from the decay of the initial ^{238}U incorporated in the lattice of the material but from external sources, such as dust or clay present as small particles in the carbonate, may bias the age determination. In addition, open-system behaviours such U leaching can occur. All these processes likely affect the sample in a heterogeneous manner[3] and may alter the apparent age of carbonate formation, which is detrimental to dating.

Until now, the direct U/Th dating with laser ablation inductively coupled plasma mass spectrometry (LA-ICPMS) has been restricted to samples with high U contents[4]. Recent advances have opened new perspectives, for example by making possible the detection of U incorporation and its heterogeneity in small carbonate samples[3]. Thanks to the spatial resolution of current lasers, it is theoretically possible to measure ^{230}Th/^{234}U ratios at the scale of about ten microns. However, such a high spatial resolution analysis is quite challenging as it involves the use of small beam diameters that consequently ablate only small quantities of material (typically few ng.s^{-1} to up to few µg.s-1 for the most efficient lasers) then limiting the counting statistics. In addition, as mentioned above, the ultra-low levels of U and ^{230}Th in some bio-carbonates make accurate quantification even more

difficult. Nevertheless, the combination of femtosecond lasers, allowing both high-resolution sampling and efficient particle transport to the ICPMS[5,6,7], with high sensitivity sector field ICPMS, now offers possibilities of few tenth of micrometer of resolution for U and Th isotope mapping while conserving a reasonable counting statistic.

In this paper, we present a new approach for direct U/Th dating of different materials using a femtosecond laser ablation coupled to a sector-field-ICPMS (fsLA-single collector ICP-SFMS) imaging. It first consists in a careful optimization of the coupling in order to improve stoichiometric U and Th transmission in the mass spectrometer and signal-to-noise ratio. In a second step, image processing is performed to identify at the micrometer scale contaminated and leached areas and determine the correction for detrital incorporation. Analyses performed on carbonates previously dated with the conventional approach are used for controlling the absence of any bias induced either during sampling, or analysis in the ICPMS. It is followed by applications to heterogeneous archaeological samples that are usually considered unsuitable for conventional U/Th dating.

EXPERIMENTAL

SAMPLES AND REAGENTS

Two speleothem samples, Salam12 and BCOH1, were used as intra-laboratory references in order to assess reliability and accuracy of our methodology. They originate from Salamandre cave[8] and Buca Cava dell'Onice cave[9] and were selected for their low U contents (167.6 ± 0.1 $ng.g^{-1}$ and 44.14 ± 0.03 $ng.g^{-1}$, respectively). They have been previously dated using the conventional U/Th approach[2]. Their ages are 104.32 ± 0.83 ka for Salam12 and 84.29 ± 0.85 ka for BCO1H. Fragments of 125 mg of Salam12 and 706 mg of BCO1H were selected for the fsLA-ICPMS analyses.

Two archaeological samples from south-african sites, a giant terrestrial snail shell (GTSS) fragment identified as BRSA9, originating from Bushman Rock Shelter[10], and a burnt ostrich eggshell (OES) fragment designated as DRS 10, originating from Diepkloof Rock Shelter[11,12] were also analyzed. They were embedded in araldite resin (araldite DBF CH Escil, Chassieu, France) and polished with diamond papers of decreasing grain diameter (P 240, P 1200) (Escil, Chassieu, France). Their U contents measured by fsLA-single collector ICP-SFMS are within the range of a few $ng.g^{-1}$ to a few tens of $ng.g^{-1}$. The sediment strata in which they have been discovered have been dated in parallel by luminescence methods. The sediment in which BRSA9 comes from was dated at 97 ± 20 ka using K-feldspar Infra-Red Stimulated Luminescence and 75±14 ka using quartz Optically Stimulated Luminescence[11], respectively designated as feldspar age and quartz age. The sediment in which DRS10 was found has been dated by two laboratories, at 52 ± 10 ka[13] and between 49 ± 5 ka and 61 ± 6 ka[14].

In addition, a U Standard Solution (USS) of 0.02 µg L^{-1} was prepared from IRMM 184 SRM (IRMM, Geel, Belgium) in 2% HNO_3 (Ultrex, Baker) diluted in ultra-pure water (Milli Q, Millipore) with 0,1% $CaCO_3$ (Suprapur, Merck Darmstadt, Germany). This solution contained a certified $^{235}U/^{238}U$ isotope ratio of $(7.2623 \pm 0.0022).10^{-3}$ and was used for mass bias correction.

INSTRUMENTATION

A 257 nm femtosecond laser ablation system delivering 360 fs pulses was used (Lambda 3, Nexeya SA, Bordeaux, France). This system can be operated within a wide range of repetition rates, from 1 Hz to 100 kHz. It features 2 galvanometric mirrors allowing rapid scanning of the beam at the sample surface which, when combined with the high laser shot frequency, allows increasing the ablation rate[15]. In this study a 10 µm laser beam diameter delivered at a repetition rate of 1 kHz was continuously and rapidly moved (1 $mm.s^{-1}$) according to a vertical back and forth movement of 40 µm while the sample was moved horizontally at a speed of 30 $µm.s^{-1}$, then resulting in 50 µm wide ablation lines. Images were obtained by ablating the samples according to successive linear ablation spaced by 50 µm (center to center). The cell washout time was assessed to be 1 s considering the 99% criterion.

A High Resolution ICPMS (Element XR, Thermo Scientific, Bremen, Germany) fitted with the Jet Interface (Thermo Scientific, Bremen, Germany) was used for detection. The laser was coupled to the ICPMS in a wet plasma configuration by means of a modified three-inlet cyclonic spray chamber that allows the dry aerosol from the ablation cell to be mixed axially upstream of the injector with the wet aerosol from the nebulization. The third inlet, tangential to the position of the nebulizer, was used to introduce a 10 ml nitrogen flow into the argon stream to get the best performance from the jet interface option. During ablation, a solution containing 2% HNO_3 diluted in ultra-pure water was nebulized in the spray chamber, while during the mass bias calibration procedure, the laser was stopped and the USS was nebulized in the spray chamber.

The fsLA-ICPMS coupling was tuned daily with a NIST 612 glass sample in order to obtain the best sensitivity while keeping a U/Th ratio of 1.00±0.05, then ensuring similar U and Th atomization and ion transmission. This stoichiometric detection of U and Th was checked prior each image acquisition. The detector voltage was set to the plateau value and the detector dead time was carefully adjusted before each analytical session. Since the signal of the most abundant isotope (^{238}U) never exceeded 1.3 MHz when ablating our carbonates samples, i.e. far below the 5 MHz switching value from pulse counting to analogue, the pulse counting mode was set for all isotopes. Operating conditions are summarized in Table 1.

Four isotopic images were acquired per sample. Depending on the samples, each image covers an area of 5 to 8 mm^2, representing an acquisition time ranging from 45 min to 1.5 hours. A pre-ablation was performed before each image in order to clean the surface of the sample from any dust brought during preparation or storage. The signal of each isotope was integrated during one second, resulting in images in counts per second (cps) with a pixel resolution of 30x50 $µm^2$. Under these conditions (Table 1), the ablation depth was approximately 30 µm. An optical surface profilometer Micromesure CHR150 (STIL Society, Aix en Provence, France) was used for measuring the ablation depth and volume. Blanks were measured for 30 minutes before and after each image.

MASS BIAS AND OXIDE CORRECTION

Mass bias is usually corrected by measuring under the same conditions a matrix matched standard sample before and after the sample. However, as no certified low U carbonate reference was available, we used a liquid matrix matched standard obtained by mixing 0.1% Suprapur $CaCO_3$ with 20 $ng.L^{-1}$ of U from IRMM 184 (USS) in HNO_3 2%. The carbonate concentration was adjusted so that the amount of calcium introduced via the nebulizer into the plasma matched the amount of calcium introduced into the plasma via the laser (estimated at approximatively 2,8 $µg.min^{-1}$). The USS solution was analyzed prior

and after each image in order to apply a bracketing mass calibration procedure, using an exponential law[16,17]. In these conditions, oxides levels were in the range of 1-2% and 2-4% respectively for UO/U and ThO/Th. U and Th isotopes were systematically corrected for these oxides values carefully measured prior and after each image.

Table 1: fsLA-single collector ICP-SFMS operating conditions

Laser ablation: Lambda 3 (Nexeya)	
Wavelength, Pulse duration, Energy	257 nm, 360 fs, 7 µJ
Repetition rate, laser beam diameter	1 kHz, 10 µm
Back and forth laser beam movement	50 µm at 1mm.s^{-1}
Sample advancement speed	30 µm.s^{-1}
Sampling strategy	Successive lines with 50 µm spacing (center to center)
Carrier gas	Ar, 320 ml.min^{-1}
Pre-ablation for surface cleaning	Repetition rate: 1 kHz, line scanned rectangle, 5 µm step between lines, scan speed: 200 mm.s^{-1}, 10 replicates
ICPMS: Element XR (Thermo Scientific)	
RF power	1020 W
Coolant gas flow	15.53 L.min^{-1}
Auxiliary gas flow	0.85 L.min^{-1}
Nebulizer gas flow, sample uptake	0.35 L.min^{-1}, 100µL.min^{-1}
Isotopes	^{230}Th, ^{232}Th, ^{234}U, ^{235}U, ^{238}U
Samples per peak, Mass Window, Resolution	30, 10%, LR
Detector Mode	Pulse counting
Sample time	66 ms
Acquisition rate	1 point.s^{-1}
Filter lens	14 -15 V

FsLA-ICPMS OPTIMIZATION

In order to accurately measure the isotopic ratios relevant for U/Th dating, the priority was first to maximise the signal sensitivity while keeping a complete atomisation of the laser induced particles in the argon plasma then insuring an efficient and stoichiometric detection of U and Th.

The laser used in this study allowed to deliver a high repetition rate and therefore to introduce a high quantity of material into the plasma per unit of time. Various conditions of repetition rate (from 1 kHz to 3 kHz), laser beam trajectories (from 20 µm to 500 µm) and sample advancement speed (from 1 µm.s^{-1} to 30 µm.s^{-1}) were combined and tested. For each condition, the volume ablated from a calcite sample was measured using a profile meter and the corresponding ablation rate (in ng.s^{-1}) was calculated considering a density of 2.9. The signal sensitivity was monitored from Calcium (^{43}Ca), as this element was considered to be homogeneously distributed in the carbonate, unlike U and Th. Plasma disturbances related to the mass loading were evaluated considering the ^{38}Ar signal prior and during ablation. As shown in Figure 1, the non-linear increase in the calcium signal with the ablation rate was accompanied by a drop in the argon signal. This drop reflects a significant reduction in plasma atomization efficiency, which can be as high as 40% at 1750 ng.s^{-1}. In addition, high ablation rates were found to lead to the accumulation of white deposits at the tip of the ICPMS cones resulting in a gradual decrease in ions transmission during the long measurement sessions required for imaging. Consequently, conditions with moderate ablation rate inducing ^{38}Ar drop less than 5 % and minimizing the signal drop over time due to matrix build up on the cones, were preferred (see report in Table 1).

Figure 1: Evolution of signal and plasma loading effect with ablation rate

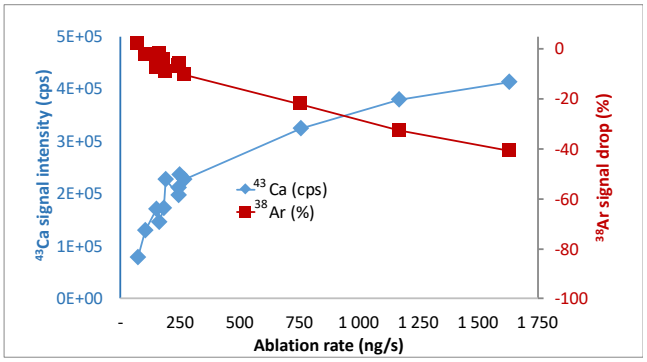

Once the compromise between robustness and signal intensity was found, around 200 ng.s^{-1}, the background signal was considered carefully. Preliminary analyses by fsLA-ICPMS of our GTSS and OES samples revealed that U concentrations were of the order of a few ng.g^{-1} to about a few tens ng.g^{-1}. These low values imply extremely low levels of ^{230}Th and ^{234}U in these samples in the order of a few tens to a few hundred fg.g^{-1}. It was then particularly important to reduce the level of the spectral background and to increase the signal to background ratio for these isotopes. Filter lens voltage was found to significantly affect background values, with a more pronounced effect for ^{230}Th. Hence, although a value of 0 V generally refers to normal conditions of use, it was found that values within a range of 14V to 15V allowed lowering significantly the signal background for all the isotopes. The background signal was reduced from 1.43 to 0.04 cps for ^{230}Th, from 324 to 14 cps for ^{232}Th, from 1.39 to 0.06 cps for ^{234}U, from 2.27 to 0.14 cps for ^{235}U and from 32.2 to 9.4 cps for ^{238}U. Although these conditions were found to induce a signal sensitivity drop of about 40% (measured from NIST612 ablation), the signal to background ratio was improved by a factor ranging from 20 for ^{230}Th to 3 for ^{238}U. In some extent, the origin of the background signal on ^{230}Th and ^{234}U might be due to the abundance sensitivity of ^{238}U and ^{232}Th and the use of the filter lens drastically minimizes this effect[18]. However, since in each isotopic image (^{230}Th, ^{232}Th, ^{234}U, ^{235}U, ^{238}U) pixels with high levels of ^{232}Th were removed during image processing (see below), only the uranium abundance sensitivity was considered here. Abundance sensitivity related to ^{238}U was measured from a 1 mg.L^{-1} uranium solution to be less than 1.10^{-8} on ^{230}Th. Note that this value is overestimated as it

includes ^{230}Th naturally occurring in the solution due to U decay. ^{231}Pa was also considered as it should be formed in the solution due to ^{235}U decay in much less extent than ^{230}Th. The abundance sensitivity was then found to be less than 5.10^{-9} which likely reflects a more representative value. Considering the low uranium signal intensity measured in our archaeological samples being less than 50000 cps on ^{238}U, the signal due to the abundance sensitivity on ^{230}Th was calculated to be less then 0.0005 cps which is at least 76 times less than the background signal. For this reason, abundance sensitivity correction was not further considered. Significant polyatomic interferences resulting from organics have been reported by Shen et al[19] (signals of 1-10 cps at masses 229-237) when analysing carbonate sample solutions with relatively high concentration of organics. In our case, even if the origin of the background is not well understood, memory effects from the analysis of previous organic samples cannot be excluded. Furthermore, traces of oil were observed at the outlet of the backing pump up to the inlet of the turbomolecular pump during a maintenance operation. It is therefore possible that residual traces of oil vapour originating from the backing pump might be partially ionised downstream of the plasma during interaction with the transmitted ion beam. However, these analytical conditions allowed to achieve very low background levels suitable for the detection of ultra-low ^{230}Th levels. Depending on the analysed samples, ^{230}Th net signals (after background correction) of 0.04 to 1.4 cps were measured, insuring a signal to background ratio above 2.

IMAGE PROCESSING

The objective of the isotopic images processing is to identify Regions Of Interest (ROIs) that are suitable for U/Th dating in contrast to ROIs exhibiting evidence of contamination and/or U leaching, unsuitable for dating. The images processing was performed using the free ImageJ software[20,21].

In a first step, the areas dominated by sediment or dust contamination had to be identified and excluded from analysis. In contrast to the speleothem samples that were well characterized and dated[22], no threshold value for the ^{232}Th/^{238}U ratio is known for the OES or GTSS samples due to the lack of empirical data about ^{232}Th contamination in these types of samples. In our samples, heterogeneous areas with high ^{232}Th/^{238}U ratio compared to the rest of the images were easily observable and morphologically identified as cracks, or surface deposits at the interface between the sample and resin. However, a threshold value of ^{232}Th/^{238}U didn't appear to be a robust criterion because of the heterogeneity of the U content in the samples: equally high ^{232}Th/^{238}U ratios can be observed in areas with the lowest U content. Instead of the direct ^{232}Th/^{238}U ratio, the higher heterogeneity of suspected detrital dominated areas was exploited for defining a different threshold criterion: these areas are characterized by higher variance values (calculated for each pixel as the variance of adjacent pixel values, meaning approximatively 1 mm^2) on the ^{232}Th/^{238}U ratio mapping. Although more samples are needed to improve this threshold definition, variance thresholds values of 1 and 2 for the ^{232}Th/^{238}U ratio were set for respectively the OES sample and the GTSS sample as a first approximation. This criterion was found to be efficient in ruling out areas with dominant detrital incorporation, and in the future its robustness will be assessed when more data are available. It is noticeable that for samples with significant detrital incorporation such as biocarbonates, this step could not remove all trace of it. Mild contaminations in remaining analysed areas were corrected by isochrone and iterative regression method, as described thereafter.

The second step consisted in detecting possible evidence for U leaching. In a closed system, the ^{234}U/^{238}U activity ratio is supposed to be homogeneous in the sample because originating from a unique source of U. However, in samples or sample areas that are not closed, U leaching can occur and makes the dating impossible, as we ignore the quantity of U that was removed. Usually, ^{234}U and ^{238}U are leached at different rates, resulting in observable variations in the ^{234}U/^{238}U activity ratio[23]. In addition, the U leaching induces an increase in the ^{230}Th/^{234}U activity ratio. Therefore, the correlation of significant changes of these ratios can be considered as an indication of leaching. Different ROIs corresponding to different ^{238}U intensities were created using the signal intensity histogram (Supporting Information, Figures S-1, S-2 and S-3). This action was facilitated by the application of a median filter of 3 pixels radius, smoothing the homogeneous areas and enhancing the contrast between areas of different signal intensity. Mask of the defined ROIs were created and applied on the initial unfiltered images for integrating the measured signals and calculating the ^{234}U/^{238}U and ^{230}Th/^{234}U activity ratios. ROIs showing significant variation of ^{230}Th/^{234}U and ^{234}U/^{238}U ratios were suspected of U leaching and removed from further analysis (Supporting Information, Figure S-4). Only few ROIs of DRS10 were concerned; no evidence of leaching was observed on the other samples.

Finally, ROIs corresponding to different areas of stable ^{232}Th/^{238}U ratios were defined using the different intensity groups identifiable on the intensity histograms of the ^{232}Th/^{238}U (Supporting Information, Figures S-5, S-6 and S-7). This identification was also facilitated by the application of the median filter. It is noticeable that the determination of these different ROIs does not affect the apparent age calculation itself, that is constant whatever the ROIs are, but has a significant impact on the accuracy of the detrital correction (see *Results* section) and therefore on the accuracy of the corrected age.

AGE CALCULATION AND UNCERTAINTIES

The total number of counts was integrated per isotope and per ROI and used to calculate the isotopic ratios, converting each ROI into a datapoint for each ratio (Supporting Information, Table S-1). Standard deviation (SD) on the background and on the raw measurements were calculated as the square root of the counts number. The quadratic sum of the absolute SD was used for uncertainty propagation related to the background subtraction. For the oxide and mass bias corrections, as for the activity ratio calculation, relative SD were summed quadratically. Average isotopic ratios were calculated from uncertainty weighted means over the different ROIs. Significant detrital contributions of ^{230}Th and ^{234}U can be present in the sample, resulting from the incorporation of detrital particles during the formation of the calcite or its burial. The time of incorporation of the detrital fraction is unknown, as well as the state of equilibrium of the U-series elements that it contains (even if it is usually assumed that the detrital U-series is at secular equilibrium). Therefore, the addition of these isotopes that are not resulting from the decay of the ^{238}U initially incorporated introduces a bias to the age calculation that can result into a significant increase of the apparent age[22]. Detrital corrected ^{230}Th/^{234}U and ^{234}U/^{238}U ratios were calculated using isochrone plots[24] based on the ROIs datapoints. This method uses ^{232}Th (which is not part of the ^{238}U series) as an estimator of the detrital contamination. It consists in plotting respectively the ^{230}Th/^{232}Th ratio against the

$^{234}U/^{232}Th$ ratio for the detrital ^{230}Th correction and the $^{234}U/^{232}Th$ ratio against the $^{238}U/^{232}Th$ ratio for the detrital ^{234}U correction. A regression method is then applied to these two datasets; the detrital $^{230}Th/^{232}Th$ and $^{234}U/^{232}Th$ parts are given by the intercept of the regression curve with the corresponding ordinate axis and the corrected $^{230}Th/^{234}U$ and $^{234}U/^{238}U$ ratios are given by the slope of the regression curve. The uncertainty on the detrital part and the uncertainty on the detrital corrected activity ratio are calculated as the standard error of the intercept and the standard error of the slope, respectively, multiplied by the appropriate critical value of the t-distribution considering a degree of freedom of n-2 (n being the number of ROIs). The isochrones curves were obtained considering all the ROIs from the different analyses for each samples as individual datapoints and using a robust iterative regression process with the Tukey's bisquare function[25,26], implemented in the Robustreg R package (https://CRAN.R-project.org/package=robustreg[27]). Ages were calculated from both error weighted mean $^{230}Th/^{234}U$ and $^{234}U/^{238}U$ activity ratios from the different ROIs, as well as for detrital ^{230}Th corrected $^{230}Th/^{234}U$ activity ratios from the isochrone regression. In order to consider uncertainties on $^{230}Th/^{234}U$ and $^{234}U/^{238}U$ ratios, age distributions were computed by 10^6 Monte-Carlo samplings of $^{230}Th/^{234}U$ and $^{234}U/^{238}U$ activity ratios[22], assuming for each sample a distribution of uncertainty according to a Student's t-distribution based on the number of degree of freedom of the model used to calculate these activity ratios. The degree of freedom is respectively calculated as n-1 and n-2 for the error weighted mean calculated ratios and for the ratios calculated from the isochrone regression. The final uncertainties on the ages were estimated at the 95% CL from the minimum and maximum ages corresponding to extrema of the 2.5% - 97.5% interval of the cumulated probability of their distribution. The Java code for Monte Carlo calculation of U/Th age, which runs as an ImageJ macro, is provided in Supporting Information, Code S-1. The age distributions calculated using this code are presented in Supporting Information, Figure S-8.

RESULTS

SPELEOTHEM SAMPLES

Despite the macroscopic homogeneity of the samples, significant variations of U content were observed on the ^{238}U images under the millimetre scale (Supporting Information, Figures S-9 and S-10). For BCO1H, the ^{238}U distribution pattern reminds those of the trigonal crystal system of calcite. These spatial variations could be related to diagenesis phenomena, to different U contents in different crystals, or to a preferential ablation efficiency depending on the crystal orientation relative to the laser beam. ROIs corresponding to different ^{238}U signal areas were created, leading to a total of 7 ROIs for Salam12 and 8 ROIs for BCO1H from the 4 images recorded for each sample. No evidence of U leaching was detected, and no significant variations of apparent ages have been observed for the different ROIs of each sample.

Measured activity ratios are summarized in Table 2, and details on each ROI are provided in Supporting Information, Table S-1. These ratios are consistent with the reference activity ratios obtained using the conventional approach, although they are less accurate. The calculated ages, respectively 100 ± 8 and 86 +11/-10 ka for Salam12 and BCO1H at the 95% CL, are in good agreement with the reference uncorrected ones (104.32 ± 0.83 and 84.29 ± 0.85 ka). The reference ages were corrected from detrital Th assuming a standard $^{230}Th/^{232}Th$ ratio of 1.25 ± 0.63: the corrected ages are 103.8 ± 1.07 and 83.04 ± 1.46 for Salam12 and BCO1H. By applying a similar correction to the data obtained by LA-ICPMS, the corrected ages are 100 +9/-8 for Salam12 and 82 +12/-10 ka for BCO1H and agree with the ages obtained with the conventional approach. With the LA-ICPMS approach, it is also possible to correct from detrital fraction incorporation using the isochrone method. The corrected age for BCO1H is 71 +44/-31 ka, and remains compatible with both previously ages corrected using the standard $^{230}Th/^{232}Th$ ratio, but is rather inaccurate. The high uncertainty results from the proximity and clustering of the isotopic ratios that penalize the isochrone regression (Supporting Information, Figure S-12). In other words, the sample is not heterogeneous enough to allow calculating a precise correction using an isochrone method. The isochrone corrected age of Salam12 is 112 ± 4 ka (older than the uncorrected one). In this case, the significant difference of ^{232}Th in the different ROIs and the good fitting of the linear regression result in an improvement of the precision. However, the y-intercept of the isochrone curve indicates a negative $^{230}Th/^{232}Th$ detrital ratio and an unusually high $^{234}U/^{232}Th$ detrital ratio (77 ± 65), while this ratio is < to 3 for BCO1H and < 1 for the shell samples (Supporting Information, Figure S-11). Even if we cannot exclude an unusual detrital fraction in this sample, it seems more reasonable to consider the possibility of a contamination during the preparation or analysis, or the fact that the isochrone correction induces a lack of accuracy for homogeneous and low ^{232}Th samples. In fact, the accuracy of the results deduced from the uncorrected LA-ICPMS measurements seems to support this conclusion.

Table 2: Summary of the measurements on speleothems

Sample	Salam12	BCO1H
Estimated Sampled mass (mg)*	1.1	1.2
Estimated U content ($ng.g^{-1}$)	168	44
Total number of ^{230}Th ions detected per sample	3703	1157
$^{230}Th/^{232}Th$	666-1252	15-72
$^{230}Th/^{234}U$	0.60 ± 0.03 Ref: 0.618 ± 0.002	0.55 ± 0.05 Ref: 0.539 ± 0.002
$^{234}U/^{238}U$	1.02 ± 0.02 Ref: 1.036 ± 0.001	1.11 ± 0.12 Ref: 1.016 ± 0.002
Age (ka)	100 +9/-8 Ref: 104.3 ± 0.8	86 +12/-11 Ref: 84.3 ± 0.9

Uncertainties are provided with a 95% CL; Isotope ratios are expressed in activity (in $Bq.Bq^{-1}$).

"Ref" refers to the conventional U/Th approach.

* Estimation based on 30µm deep ablation and carbonate density of $2.6g.cm^{-3}$

From all these analyses, it appears that, despite larger uncertainties compared to the conventional approach, our method is reliable for measuring isotopic ratios, even from small amounts of low U carbonates. In particular, these results demonstrate that

no uncorrected bias which might affect the measurement of natural U and Th isotopes is induced neither during the laser sampling, nor during the measuring process.

ARCHAEOLOGICAL SAMPLES

Images from BRSA9 show layered variations of ^{238}U and ^{232}Th intensities (Figure 2). A similar U distribution, correlated with the shell layered structure, has been observed for marine shells[28]. DRS10 exhibits a more homogeneous U content, lower on the external part of the sample (Figure 3), but without specific incorporation patterns such those observed by Sharp et al.[3] on unburnt OES samples. For DRS10, the ^{232}Th distribution is heterogeneous with a low $^{230}Th/^{232}Th$ ratio, suggesting a high Th contamination (Figure 3). A total of 20 and 13 ROIs were then defined for BRSA9 and DRS10, respectively. A few ROIs attesting contamination from the surrounding sediment or dust (high ^{238}U and ^{232}Th signals, and high $^{232}Th/^{238}U$ ratios) were spotted on BRSA9 and DRS10 images, likely corresponding to cracks in the samples. Evidences of leaching were found in few low U ROIs in DRS10 (Supporting Information, Figure S-4), that were then discarded before age calculation.

Figure 2: BRSA9 ^{238}U and ^{232}Th images of BRSA9 Internal side of the seashell facing up

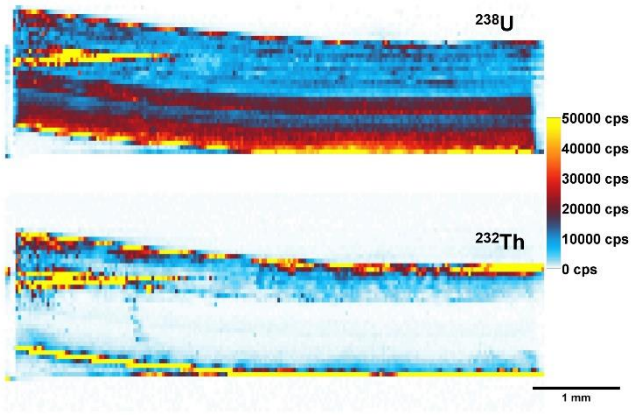

Figure 3: ^{238}U and ^{232}Th images of DRS10 Internal side of the eggshell facing up

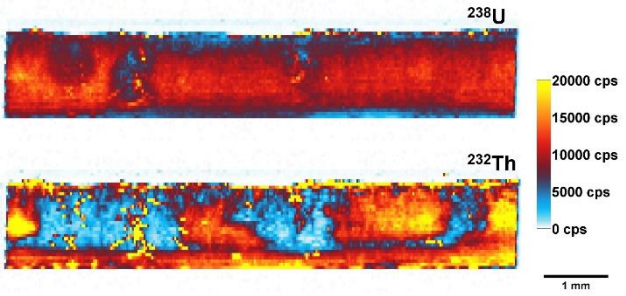

Figure 4: Isochrone plots of BRSA9 measurements
a - Isochrone plot of $^{230}Th/^{232}Th$ by $^{234}U/^{232}Th$

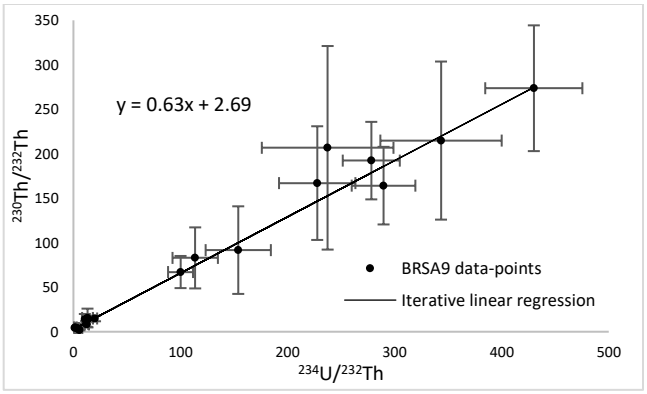

b - Isochrone plot of $^{234}U/^{232}Th$ by $^{238}U/^{232}Th$

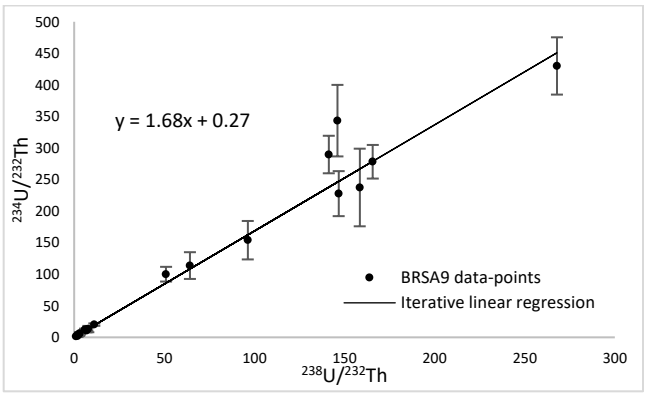

Figure 5: Isochrone plots of DRS10 measurements
a - Isochrone plot of $^{230}Th/^{232}Th$ by $^{234}U/^{232}Th$

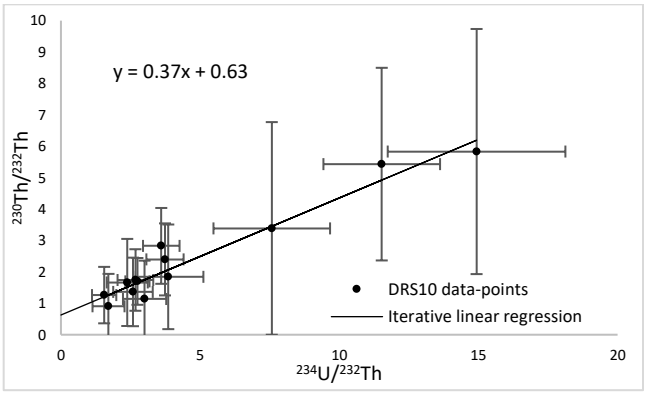

b - Isochrone plot of $^{234}U/^{232}Th$ by $^{238}U/^{232}Th$

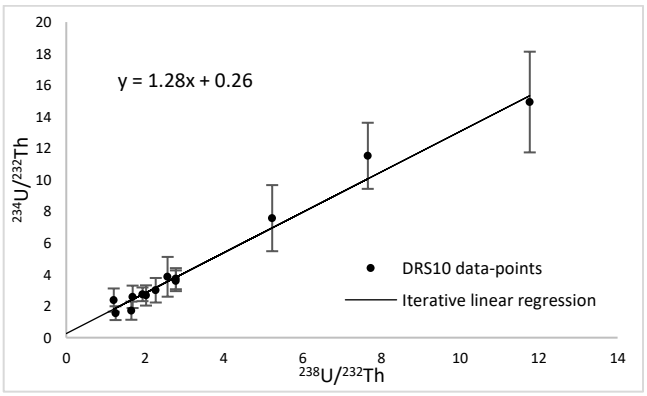

Table 3: Summary of the measurements on shell samples

Sample	BRSA9	DRS10
Estimated Sampled mass (mg)*	1.95	1.40
Estimated U content ($ng.g^{-1}$)	10-30	1-10
Total number of ^{230}Th ions detected per sample	776	197
$^{230}Th/^{232}Th$	2-290	1-6
detrital $^{230}Th/^{232}Th$	3 ± 4	0.6 ± 0.4
Uncorrected $^{230}Th/^{234}U$	0.71 ± 0.06	0.56 ± 0.11
Detrital corrected $^{230}Th/^{234}U$	0.63 ± 0.03	0.37 ± 0.07
Uncorrected $^{234}U/^{238}U$	1.74 ± 0.12	1.37 ± 0.11
Detrital corrected $^{234}U/^{238}U$	1.68 ± 0.02	1.28 ± 0.11
Uncorrected age (ka)	119 +50/-36	86 +20/-17
Detrital Th corrected age (ka)	100 ± 6	50 +13 /-11
Luminescence age of strata (ka)	97 ± 20 (feldspar age) 75±14 (Quartz age)[10]	52 ± 10 [13]; 49 ± 5 to 61 ± 6 [14]

Uncertainties are provided with a 95% CL – Isotope ratios are expressed in activity (in $Bq.Bq^{-1}$).

* Estimation based on 30µm deep ablation and carbonate density of $2.6g.cm^{-3}$

The activity ratios are summarized in Table 3 and details for each ROI are provided in Supporting Information, Table S-1. The isochrone provided a good fit to the BRSA9 data-points (Figure 4), resulting in a significant improvement in the age uncertainty. The detrital corrected age, 100 ± 6 ka, is compatible with the feldspar age (97 ± 20 ka) but not with the quartz age (75±14 ka)[10] . The difference between quartz age and feldspar age – which are just compatible to each other – is discussed in Porraz et al.[10] but the reasons for this discrepancy are unclear. For DRS10, a significant contribution of detrital ^{230}Th can be suspected considering the very low $^{230}Th/^{232}Th$ activity ratios, lower than 10 in all ROIs, what was confirmed by the isochrone analysis (Figure 5.a). Detrital ^{230}Th correction allowed calculating a $^{230}Th/^{234}U$ ratio and a U/Th age significantly lower than the uncorrected one. An improvement of the uncertainty resulted from the good fitting of the data-points with the regression, despite the large uncertainty on each individual data-point value. The corrected age of DRS10, 50 +13/-11 ka, is consistent with the luminescence ages reported by Tribolo et al.[13] (52 ± 10 ka) and by Jacobs and Roberts[14] (between 49 ± 5 ka and 61 ± 6 ka). The detrital corrections of the $^{234}U/^{238}U$ ratios (Figure 4.b and Figure 5.b), although not negligible, had no significant impact on the age value calculated for both shell samples. Still, the isochrone method allowed a improvement of the uncertainty of this ratio for BRSA that benefited to the age accuracy.

DISCUSSION

The good consistency of the activity ratios and U/Th ages obtained for speleothem samples using the conventional approach and the presented methodology indicates the reliability and accuracy of the latter. Nevertheless, it is obvious that supplementary analyses are required for investigating the limits of this approach. At present, the age uncertainties are significantly higher than those obtained when usual U/Th dating using liquid preparation and MC-ICPMS analysis are applied: with the fsLA-single collector ICP-SFMS approach, the uncertainties range from 6% to 22% (95% CL), a value which strongly depends on the ^{230}Th content and on the accuracy of the detrital correction. It also strongly depends on the counting statistics which is directly related with the ionic transmission of the ICPMS and the sample mass used for the analysis (which is about 2 orders of magnitude less with our approach compared to the conventional one). The sequential detection of single collector ICP-SFMS also affects the counting statistics compared to multicollection detection. Further improvement of our approach would certainly rely on high transmission fsLA-MCICPMS. It is noticeable that the previous attempt done by Spooner et al.[4] on samples with U contents higher than 4 $µg.g^{-1}$ provided measurements with an equivalent uncertainty. However, their objective was only to perform fast age screenings (10 to 20 times shorter than the presented protocol) for sampling guidance. fsLA-single collector ICP-SFMS imaging provides additional high-resolution data for U and Th distributions, with a better detection threshold: it consequently enables LA-ICPMS dating of low U carbonates while allowing accurate detrital corrections by combining isotopic imaging and image processing. This improvement is at the cost of longer analyses and data processing times, and necessitates high ablation efficiency and high detection sensitivity ICPMS which are not achievable with common LA-ICPMS systems.

The U/Th ages of the GTSS and the burnt OES are consistent with those obtained by luminescence methods for the corresponding strata. They are exploitable in the context of archaeological investigations even though their uncertainties are not as low as the typical uncertainty obtained with the bulk conventional double spike and MC-ICPMS U/Th analysis on well preserved samples. However, this image processing approach allows separating contaminated and leached areas from exploitable ROIs, and correcting for detrital ^{230}Th contamination, what would not have been possible with the conventional approach as samples are digested and homogenised. It is also noticeable that the sampled mass is about two orders of magnitude smaller than what is required for the conventional approach, which makes it suitable for very small samples, even in the case of high detrital contamination.

Despite significant internal variations of the U content for both GTSS and burnt OES samples, no apparent internal age variation was observed. This observation supports the hypothesis that these types of shells behave mostly like closed systems, or at least, they only experienced a fast and single incorporation event. It is of particular interest for OES because previous studies on raw or less heated samples highlighted significant and progressive secondary incorporation[3], that yielded, at best, minimum ages or burial ages through U incorporation models (at the cost of additional hypotheses). The burning of the OES sample might have induced a closure of the system with respect to U incorporation, in addition to the elimination of organic tissues, disintegration of the mammillary layer cones part of the shell and structural changes in the palisade layer[29]. According to experimental burning of modern OES fragments, this necessitates a temperature of at least 450°C that is achievable inside utilitarian fires only when fragments are at a maximum depth of 2 cm below the ground surface[30]. It is therefore likely that the burning of this type of samples is contemporary of their burial. If this hypothesis is confirmed by further analyses, burnt OES could be a material of choice for U/Th dating.

In contrast to what is usually observed with the conventional approach, the detrital correction applied here using the isochrone method may lead to a significant improvement of the accuracy. Although the iterative regression calculation improves the fitting by reducing the influence of potential outliers[23,24], the major part of this gain comes from the strategy of the ROI definition. The accuracy of the slope and the intercept increases proportionally to the standard deviation of the variable distribution (abscissa), i.e. the $^{234}U/^{232}Th$ ratio or $^{238}U/^{232}Th$ ratio. Defining ROIs based on the $^{232}Th/^{238}U$ ratios creates datasets with the highest variation between $^{234}U/^{232}Th$ values and between the $^{238}U/^{232}Th$ values, what optimizes the accuracy of the regression in the case of an effective correlation of apparent age with detrital ^{232}Th (Figure 4 and Figure 5). This benefit is higher with heterogeneous sample with high detrital fraction but may be too limited to counterbalance the additional uncertainty from the ^{230}Th detrital correction in more homogeneous samples, or in samples poor in detrital fraction such as BCO1H. As this method requires to define sub-samplings according to U and Th isotopes variations, it obviously necessitates high-resolution isotopic imaging and image processing, what is possible with a LA-ICPMS mapping approach but not with the conventional sample nebulisation approach.

The sample throughput is not shorter with this methodology than with the conventional approach. The later allows preparing and measuring a whole series of samples while only one sample at a time can be analysed with a laser ablation protocol. Although the sample preparation is faster with the fsLA-single collector ICP-SFMS approach, the time of analysis and the time required for data processing is longer. The ablation of one sample itself can take from half an hour to two hours, and at least one additional half hour is necessary for background measurements. The image processing for one analysis may vary from one to three hours, depending on the complexity and state of alteration of the sample. Considering that several images are required for increasing the counting statistic, the time required for analysing and dating a single sample may reach a few days.

CONCLUSION

The femtosecond laser ablation–single collector ICP-SFMS approach enables the U-Th dating of small, low U and altered samples, using a protocol which requires no chemical preparation but exploits the analysis of isotopic images. The ages obtained for two reference speleothem samples were found to be consistent with the ages obtained using the conventional approach. For two archaeological shell samples, the detrital corrected U/Th ages have uncertainties similar or higher to that of luminescence ages and are consistent with the luminescence based chronology of the sediment strata. The small quantity of matter required with our approach together with the high spatial resolution and the possibility to correct for contaminations, makes this approach interesting for the U/Th dating of small carbonate samples that are not datable with standard protocols. In archaeology, these analytical developments are of great potential as they represent new sampling strategies for getting ages with the U-Th dating method.

ASSOCIATED CONTENT

Supporting Information

Age equation of the U/Th dating method: Formula S-1. Figures S-1 and S-2 detailing the different steps for defining the ^{238}U based ROIs using the ^{238}U distribution histogram (Figure S-3). Graph of the results of an analysis with suspected uranium leaching: Figure S-4. Figures S-5 and S-6 detailing the different steps for defining the $^{232}Th/^{238}U$ based ROIs using the $^{232}Th/^{238}U$ distribution histogram (Figure S-7). Isotopic ratio measured on each ROI for the different samples: table S-1. Monte Carlo code of the ImageJ macro for calculation of a U/Th age: Code S-1. Age distributions of the samples: Figure S-8. ^{238}U and ^{232}Th mappings of the speleothem samples: Figures S-9 and S-10. Isochrone plots of the speleothem samples: Figures S-11 and S-12.

AUTHOR INFORMATION

Corresponding Authors

* christophe.pecheyran@univ-pau.fr

* loic.martin@glasgow.ac.uk

Author Contributions

The manuscript was written through contributions of all authors. All authors have given approval to the final version of the manuscript.

ACKNOWLEDGMENT

The authors are grateful to the Région Nouvelle-Aquitaine and to the ANR that funded these researches (including post-doctoral funding for Loïc Martin) through the projects DAPRES LA FEM, ANR DOM-ART, and ANR APART (grant number ANR 18-CE 27 - 0004) and its project leaders that participated to the development of the method. We are thankful to N. Brutel and M. Taris that worked on samples analysis and on methodological developments. We are grateful to D. Lelièvre from providing the sample from Salamandre cave (France) and to I. Isola for providing the sample from Buca Cava dell'Onice (Italy). F. Thil and A. Dapoignny are also thanked for their assistance during BCO and Salam analysis by MC-ICPMS. We thank the South African Heritage Resource Agency for the export permits of the shells (permits ID 2580 and 2706).

REFERENCES

1. Edwards, L.R.; Chen, J. H.; Wasserburg, G. J. 238U-234U_230Th- 232Th systematics and the precise measurement of time over the past 500,000 years. *Earth Planet. Sci. Lett.*, **1987**, 81, 175-192

2. Pons-Branchu, E.; Douville, E.; Roy-Barman, M.; Dumont, E.; Branchu, E.; Thil, F.; Frank, N.; Bordier, L.; Borst, W. A geochemical perspective on Parisian urban history based on U-Th dating, laminae counting and yttrium and REE concentrations of recent carbonates in underground aqueducts. *Quat. Geochronol*., **2014**, 24, 44-53

3. Sharp, W. D.; Tryon, C. A.; Niespolo, E. M.; Fylstra, N. D.; Tripathy-Lang, A.; Faith, J. T. 230Th/U burial dating of ostrich eggshell. *Quat. Sci. Rev*., **2019**, 219, 263-276

4. Spooner, P. T.; Chen, T.; Robinson, L. F.; Coath C. D. Rapid uranium-series age screening of carbonates by laser ablation mass spectrometry. *Quat. Geochronol*., **2016**, 31, 28-39

5. Donard, A.; Pottin, A.-C.; Pointurier, F.; Pecheyran, P. Determination of relative rare earth element distributions in very small quantities of uranium ore concentrates using femtosecond UV laser ablation–SF-ICP-MS coupling. *J. Anal. At. Spectrom*., **2015**, 30, 2420–2428

6. Donard, A.; Claverie, F.; Pointurier, F.; Blitz Frayret, C.; Svatosova, B.; Pecheyran, P. Direct online determination of laser-induced particle size distribution by ICPMS. *Anal. Chem.*, **2017**, 89, 8791−8799

7. Centrella, S.; Beaudoin, N. E.; Derluyn, H.; Motte, G.; Hoareau, G.; Lanari, P.; Piccoli, F.; Pecheyran, C.; Callo, J. P.; Micro-scale chemical and physical patterns in an interface of hydrothermal dolomitization reveals the governing transport mechanisms in nature: Case of the Layens anticline, Pyrenees, France. *Sedimentology*, **2020**, doi: 10.1111/sed.12808

8. Pons-Branchu, E.; Hamelin, B.; Brulhet, J.;Bruxelles, L.Speleothem rupture in karst: tectonic or climatic origin? U-Th dating of rupture events in Salamandre Cave (Gard, South-Eastern France). *Bulletin de la Société Géologique de France*, **2004**, 175, 473-479.

9. Isola, I; Ribolini, A.; Zanchetta, G.; Bini, M.; Regattieri, E.; Drysdale, R.; Hellstrom, J.; Bajo, P.; Montagna, P.; Pons-Branchu, E. Speleothem U/Th age constraints for the Last Glacial conditions over the Apuan Alps, Northwestern Italy. *Palaeogeogr. Palaeoclimatol. Palaeoecol*., **2019**, 518, pp. 62-71

10. Porraz, G.; Val, A.; Tribolo, C.; Mercier, N.; De La Peña, P.; Haaland, M. M.; Igreja, M.; Miller, C. E.; Schmid, V. C. The MIS5 pietersburg at 28' bushman rock Shelter, Limpopo Province, South Africa. *PLoS ONE*, **2018**, 13, Issue 10

11. Porraz, G.; Texier, P.-J.; Archer, W.; Piboule, M.; Rigaud, J.-P.; Tribolo, C. Technological successions in the Middle Stone Age sequence of Diepkloof Rock Shelter, Western Cape, South Africa. *J. Archaeol. Sci.*, **2013**, 40, 3376-3400

12. Steele, T. E.; Klein, R. G. The Middle and Later Stone Age faunal remains from Diepkloof Rock Shelter, Western Cape, South Africa. *J. Archaeol. Sci*., **2013**, 40, 3453-3462

13. Tribolo, C.; Mercier, N.; Douville, E.; Joron, J.-L.; Reyss, J.-L.; Rufer, D.; Cantin, C.; Lefrais, Y.; Miller, C. E.; Porraz, G.; Parkington, J.; Rigaud, J.-P.; Texier, P.-J. OSL and TL dating of the Middle Stone Age sequence at Diepkloof Rock Shelter (South Africa): a clarification. *J. Archaeol. Sci*., **2013**, 40, 3401-3411

14. Jacobs, Z.; Roberts, R. G. An improved single grain OSL chronology for the sedimentary deposits from Diepkloof Rockshelter, Western Cape, South Africa. *J. Archaeol. Sci*., **2015**, 63, 175-192

15. Aramendía, M.; Rello, L.; Bérail, S.; Donnard, A.; Pécheyran, C.; Resano, M. Direct analysis of dried blood spots by femtosecond-laser ablation-inductively coupled plasma-mass spectrometry. Feasibility of split-flow laser ablation for simultaneous trace element and isotopic analysis. *J. Anal. At. Spectrom.*, **2015**, 30, 296-309

16. Russell W. A.; Papanastassiou D. A.; Tombrello T. A. Ca isotope fractionation on the Earth and other solar system materials. *Geochim. Cosmochim. Acta*, **1978**, 42, 1075–1090.

17. Claverie, F; Hubert, A; Berail, S; Donard, A; Pointurier, F; Pecheyran, C; Improving precision and accuracy of isotope ratios from short transient Laser Ablation – Multi-Collector-ICPMS signals: application to micron-size uranium particles. *Anal. Chem*., **2016**, 88, 4375-4382

18. Prohaska, T.; Irrgeher, J.; Zitek, A.; Jakubowski, N.; Sector Field Mass Spectrometry for Elemental and Isotopic Analysis. *Royal Society of Chemistry*, **2014**, pp 77-78

19. Shen, C.-C.; Edwards, R. L.; Cheng, H.; Dorale, J. A.; Thomas, R. B.; Moran, S. B.; Weinstein, S. E.; Edmonds, H. N. Uranium and thorium isotopic and concentration measurements by magnetic sector inductively coupled plasma mass spectrometry. *Chem. Geol*., **2002**, 185, 165– 178

20. Abràmoff, M. D.; Magalhães, P. J.; Ram, S. J. Image Processing with ImageJ. *Biophotonics Int*., **2004**, 11, 36-42

21. Rasband, W. S. ImageJ, U.S. National Institutes of Health, Bethesda, Maryland, USA, **1997** – **2012**, imagej.nih.gov/ij/

22. Bourdon, B.; Henderson, G. M.; Lundstrom, C. C.; Turner, S. P. Uranium-series geochemistry. *Rev. Mineral. Geochem*., 52, Geochemical Society, Mineralogical Society of America, 2003

23. Yehuda, E.; Fleischer, R. L. Preferential leaching and the age of radiation damage from alpha decay in minerals. *Geochim. Cosmochim. Acta*., **1985**, 49(5), 1155-1164.

24. Bischoff, J. L.; Fitzpatrick, J. A. U-series dating of impure carbonates: an isochron technique using total-sample dissolution. *Geochim. Cosmochim. Acta*., **1991**, 55(2), 543-554.

25. Birch, J. B. On the power of robust tests in analysis of covariance. Commun. Stat. - Simul. Comput., 1983, 12, 159-182

26. Huber, P. J. John W. Tukey's Contributions to Robust Statistics. *Ann. Stat*., **2002**, 30, 1640-1648

27. R Core Team. R: A Language and Environment for Statistical Computing. R Foundation for Statistical Computing, Vienna, Austria, **2019** https://www.r-project.org (accessed Sept 3, 2019)

28. Helama S.; Heikkilä, P.; Rinne, K.; Kresten Nielsen, J.; Kresten Nielsen, J. LA-ICP-MS-derived U-concentrations and microstructural domains within biogenic aragonite of Arctica islandica shell. *Environ. Monit. Assess*., **2015**, 187, 260

29. Collins, B.; Steele, T. E. An often-overlooked resource: Ostrich (Struthio spp.) eggshell in the archaeological record. *J. Archaeol. Sci.* **2017**, Reports 13, 121–131

30. Werts, S.P.; Jahren, A.H. Estimation of temperatures beneath archaeological campfires using carbon stable isotope composition of soil organic matter. *J. Archaeol. Sci*., **2007**, 34, 850-857

For Table of Contents Only